Available online at www.sciencedirect.com
ScienceDirect
Journal of the European Ceramic Society 28 (2008) 1715–1722
www.elsevier.com/locate/jeurceramsoc

Thermal decomposition, densification and mechanical properties of AlN–SiC(–TiB_2) systems with and without B, B_4C and C additives

Sea-Hoon Lee [a,*], Shuqi Guo [a], Hidehiko Tanaka [b], Kenji Kurashima [b], Toshiyuki Nishimura [b], Yutaka Kagawa [c]

[a] *National Institute for Materials Science, 1-2-1 Sengen, Tsukuba, Ibaraki 305-0047, Japan*
[b] *National Institute for Materials Science, 1-1 Namiki, Tsukuba, Ibaraki 305-0044, Japan*
[c] *University of Tokyo, Research Center for Advanced Science and technology (RCAST), 4-6-1 Komaba, Meguro-ku, Tokyo 153-8505, Japan*

Received 9 July 2007; received in revised form 20 November 2007; accepted 30 November 2007
Available online 19 February 2008

Abstract

Thermal decomposition of AlN–SiC(–TiB_2) systems during densification was analyzed, and effects of B, B_4C and C on the densification behavior of the systems were studied. SiO_2 impurity in the powder mixture was nearly completely removed by carbothermal reaction at 1500 °C in vacuum, while Al_2O_3 remained and affected the densification behavior of the system. The onset temperature of densification of a AlN–SiC–TiB_2 system decreased from 2050 to 1850 °C by the addition of carbon, which decreased further (1680 °C) by adding both B_4C and carbon. Dense AlN–SiC–TiB_2 specimens were obtained after the hot pressing at 2000 °C by the application of carbon and boron or B_4C. Young's modulus, hardness, fracture toughness and thermal conductivity of a AlN–SiC–TiB_2 system sintered with B_4C and C were 313 GPa, 18.2 GPa, 3.7 MPa $m^{1/2}$ and 22.9 W/(m °C), respectively.

Keywords: SiC; AlN; Sintering; Mechanical properties; Thermal properties

1. Introduction

Silicon-based non-oxide ceramics have been intensively investigated for the application at elevated temperature. However, in the combustion environments, the practical application temperature of the ceramics has been limited to ~1100 °C due to the corrosion and evaporation of protective SiO_2 layer by the reaction with humidity, Na/K ions and sulfur.[1–3] On the other hand, more corrosion resistant mullite has been reported to survive up to 1300 °C at the same condition.[4]

Although oxidation and corrosion resistance of AlN–SiC systems are worse than those of SiC,[5] TiB_2 additive has been reported to improve the properties significantly due to the promotion of protective mullite layer formation during oxidation above 1000 °C.[6,7]

Al_2O_3, SiO_2, TiO_2 and B_2O_3 which are contained in the AlN–SiC–TiB_2 powder mixture produce liquid phases during densification due to the low eutectic temperature (*e.g.*, Al_2O_3–SiO_2–TiO_2: 1480 °C),[8] thus decrease high temperature properties of the system. Rafaniello et al. reported that AlN–SiC specimens exhibited creep resistance comparable to solid state sintered SiC above 1425 °C by adding C source (starch) in order to remove inherent silicate.[9] The result indicates that thermal decomposition analysis is required to improve high temperature properties of the AlN–SiC–TiB_2 system.

For the fabrication of dense AlN–SiC(–TiB_2) materials without sintering additives, application of high temperature (≥2000 °C) and pressure are generally required.[10] Boron, B_4C and carbon have been widely used as sintering additives of SiC.[11] However, their effects on the AlN–SiC(–TiB_2) systems have not been well understood.

Here we report the effects of boron, B_4C and carbon on the densification, microstructure and phase formation of SiC–AlN–(TiB_2) systems. Thermal decomposition reactions of the system were analyzed, and the mechanical proper-

* Corresponding author. Tel.: +81 29 859 2432; fax: +81 29 859 2401.
E-mail address: LEE.Seahoon@nims.go.jp (S.-H. Lee).

0955-2219/$ – see front matter © 2008 Elsevier Ltd. All rights reserved.
doi:10.1016/j.jeurceramsoc.2007.11.012

Table 1
Chemical composition of the systems

Abbreviation	Weight (g)					
	AlN	SiC	TiB_2	B	B_4C	Phenolic resin
AS	9.78	3.16	0	0	0	0
AST	9.78	3.16	0.68	0	0	0
ASTC	9.78	3.16	0.68	0	0	0.73
ATB4C	12.94	0	0.68	0	0.14	0.73
STB4C	0	12.94	0.68	0	0.14	0.73
ASTBC	9.78	3.16	0.68	0.14	0	0.73
ASTB4C	9.78	3.16	0.68	0	0.14	0.73

ties and thermal conductivity of the sintered systems were measured.

2. Experimental

Table 1 shows the composition of starting materials. In the abbreviation, A, S, T, B, B4 and C represent AlN (Type E, Tokuyama Corp.), α-SiC (UF-15, H.C. Starck), TiB_2 (Grade PF, Japan New Metals Co.), boron (Amorphous boron, H.C. Starck), B_4C (Grade HD20, H.C. Starck), and carbon which was derived from a phenolic resin (Phenolite J-325, Dainippon Ink Inc., ceramic yield: 37.4%), respectively.

The mole ratio between AlN and SiC was fixed to 3:1 so that the oxidized material has stoichiometric composition of mullite ($3Al_2O_3{\cdot}2SiO_2$). 5 wt% TiB_2 was added to the AlN and SiC mixture in order to enhance the formation of mullite during oxidation,[7] except for the AS system.

The AS and AST systems informed the densification behavior of AlN–SiC(–TiB_2) powder mixture without additives. Effects of carbon, boron and B_4C were analyzed by the ASTC, ASTBC and ASTB4C systems. ATB4C and STB4C systems, which did not contain either SiC or AlN, were applied to analyze the component which governed the densification behavior.

The raw materials were mixed intensively by planetary mill with ethyl alcohol at 150 r.p.m. for 4 h using SiC jar and SiC ball. The powder mixtures were dried at 70 °C with stirring and screened through a 120-mesh sieve. In order to analyze the decomposition behavior during densification, thermal gravimetric analysis (TGA, STA 409CD, Netzsch) was performed up to 1800 °C in flowing Ar using graphite crucibles (flow rate: 100 ml/min, heating rate: 10 °C/min up to 1000 °C, 3 °C/min above 1000 °C, holding for 30 min at 1500 °C).

The surface oxides on SiC, AlN and TiB_2 powder may induce liquid phase sintering of the AlN–SiC(–TiB_2) system. In order to reduce the amount of the oxides, the powder mixtures were held at 1500 °C for 30 min in vacuum (pressure: $<10^{-2}$ Pa) during the temperature increasing stage for hot pressing. The change of surface area and oxygen content of the powder mixture before and after heat treatment at 1500 °C was measured using Brunauer, Emmett, Teller method (BET, Autosorb-1, Quantachrome) and inert gas carrying melting-infrared absorptiometer (TC-600, Leco), respectively.

The powder mixtures were hot pressed (FVHP-1-3, Fuji Dempa Kogyo Corp., heating rate: 75 °C/min up to 1500 °C, 30 °C/min above 1500 °C, pressure: 20 MPa) at 1950–2200 °C for 1 h in Ar atmosphere with *in situ* monitoring of the shrinkage. The microstructure and chemical composition of the ATB4C system sintered at 1930 and 2010 °C were analyzed by a transmission electron microscope (TEM, JEM-2000EX, Jeol).

After the densification, density of the sintered bodies was analyzed using Archimedes' method. The density value used for α-SiC, AlN, TiB_2, boron and amorphous carbon was 3.16, 3.26, 4.52, 2.34 and 1.95 g/cm^3, respectively.[12,13]

The effects of sintering temperature and additive composition on the phase formation of the systems were analyzed by X-ray powder diffraction (XRD, JDX-3500, JEOL) with Cu Kα radiation.

Young's modulus, hardness and fracture toughness of the specimens were measured by the pulse echo method (5072PR, Panametrics, sample thickness: 3 mm) and Vickers indentation method (AVK-A, Akashi, loading condition: 10 kg, 15 s, 5 measurements per sample), respectively.[14,15] After indentation test, crack propagation behavior was observed using scanning electron microscopy (SEM, JSM-6700F, JEOL).

Thermal conductivity of the ASTB4C system sintered at 2100 °C was measured at room temperature using a flash diffusivity instrument (LFA 447, Netzsch). In order to minimize the effect of porosity on the thermal conductivity, the specimen was hot pressed with high pressure (45 MPa).

3. Results

3.1. Thermal decomposition

Fig. 1 shows TGA data of the systems in Ar atmosphere. The weight loss of the AS system occurred at and above 1250 °C, which continued during annealing at 1500 °C. A rapid weight loss started at about 1700 °C. TGA data of the AST system were

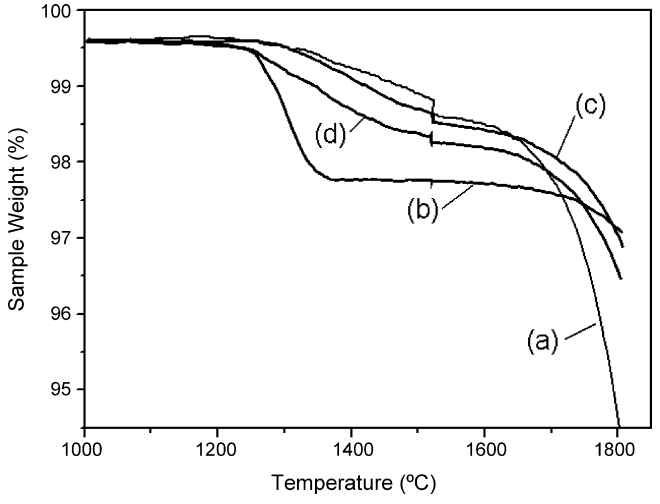

Fig. 1. TGA data of (a) AS (b) STB4C (c) ATB4C and (d) ASTB4C in Ar atmosphere (heating rate: 3 °C/min. Holding for 30 min at 1500 °C, Ar flow rate: 100 ml/min).

Table 2
Surface area and oxygen content of the AST and ASTC powder mixture before and after the heat treatment at 1500 °C in vacuum for 30 min

Properties	Powder condition			
	AST		ASTC	
	Raw powder	After treatment	Raw powder	After treatment
Surface area (m^2/g)	6.25	4.74	380.9	7.23
Oxygen content (wt%)	1.1	0.76	1.6	0.63

similar to those of the AS system, thus were not described in Fig. 1.

The STB4C system had strong mass loss above 1250 °C, which was completed at 1380 °C. Additional weight loss did not occur during annealing at 1500 °C for 30 min. In contrast to the STB4C system, the ATB4C system lost weight at 1500 °C. The weight loss of the ASTB4C system was similar to that of the ATB4C system, except a large weight loss below 1380 °C.

Table 2 shows the surface area and oxygen content of the AST and ASTC powder mixture before and after heat treatment at 1500 °C in vacuum for 30 min. The oxygen content in the ASTC system was lower than that of the AST system. The surface area of both the AST and ASTC systems decreased after annealing at 1500 °C. The surface area of the ASTC system was very high (380.9 m^2/g).

3.2. Densification and phase analysis

Shrinkage of the AS system occurred above 1600 °C, which stopped at 1850 °C (Fig. 2a). Additional shrinkage was not clearly observed above this temperature during hot pressing at 2100 °C for 1 h. However, differentiation of the shrinkage curves (Fig. 2b) indicated the presence of a minor shrinkage at 1970–2060 °C. The AS system densified during hot pressing at 2000 °C for 1 h (Table 3), while the behavior was strongly suppressed at 2100 °C (Fig. 2a, Table 3). Relative density of the specimens sintered at 2000 and 2100 °C was 91 and 67.7%, respectively.

Table 3
Relative density of samples with different composition and sintering conditions

Sintering condition	Relative density (%)	Sintering condition	Relative density (%)
AS, 2000 °C, 1 h, HP	91.0	STB4C, 2100 °C, 1 h, HP	96.9
AS, 2100 °C, 1 h, HP	67.7	ASTBC, 1950 °C, 1 h, HP	91.3
AST, 2100 °C, 1 h, HP	89.2	ASTBC, 2000 °C, 1 h, HP	98.3
ASTC, 2100 °C, 1 h, HP	98.2	ASTBC, 2100 °C, 1 h, HP	97.8
ATB4C, 2100 °C, 1 h, HP	97.7	ASTB4C, 2100 °C, 1 h, HP	98.9

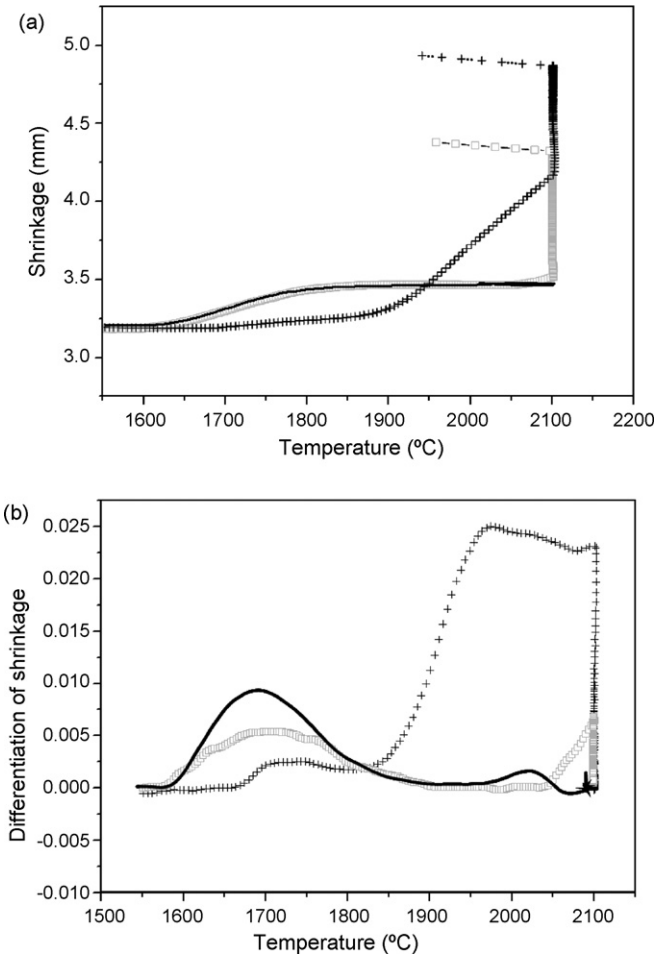

Fig. 2. (a) Shrinkage and (b) differentiation of shrinkage of samples with temperature in Ar (–: AS, □: AST and +: ASTC). The samples were heat treated at 1500 °C for 30 min in vacuum before hot pressing at 2100 °C for 1 h in Ar. The vertical lines represent densification at 2100 °C, and subsequent shrinkage can be observed during cooling (heating rate: 30 °C/min).

XRD data informed the formation of AlN–SiC solid solution after the sintering of the AS system at and above 2000 °C (Fig. 3a–c). The peak intensity of α-SiC (6H) at 35.2–35.6° decreased and the peak shifted toward that of AlN (2H) at 36° with the formation of a AlN–SiC solid solution.[16] Minute residual peak of α-SiC was observed in the AS system sintered at 2000 and 2100 °C. In spite of the formation of solid solution, densification of the AS system did not occur at 2100 °C under 20 MPa pressure.

Addition of TiB_2 in the AS system induced shrinkage above 2050 °C (Fig. 2b), which was clearly different from the AS system. Formation of solid solution was completed after the hot pressing of the AST system at 2100 °C (Fig. 3e). XRD analysis also informed the formation of BN in the AST system.

The first shrinkage at 1600 °C shown in the AST system did not occur when adding carbon (ASTC system, Fig. 2a). Sintering shrinkage of the ASTC system started at 1850 °C. Densification did not intensively occur at 1950 °C (relative density: 74.7%), but a dense specimen was obtained at 2100 °C (Table 3).

Fig. 4 shows densification of the ATB4C, STB4C, ASTB4C and ASTBC system. In contrast to the specimens without addi-

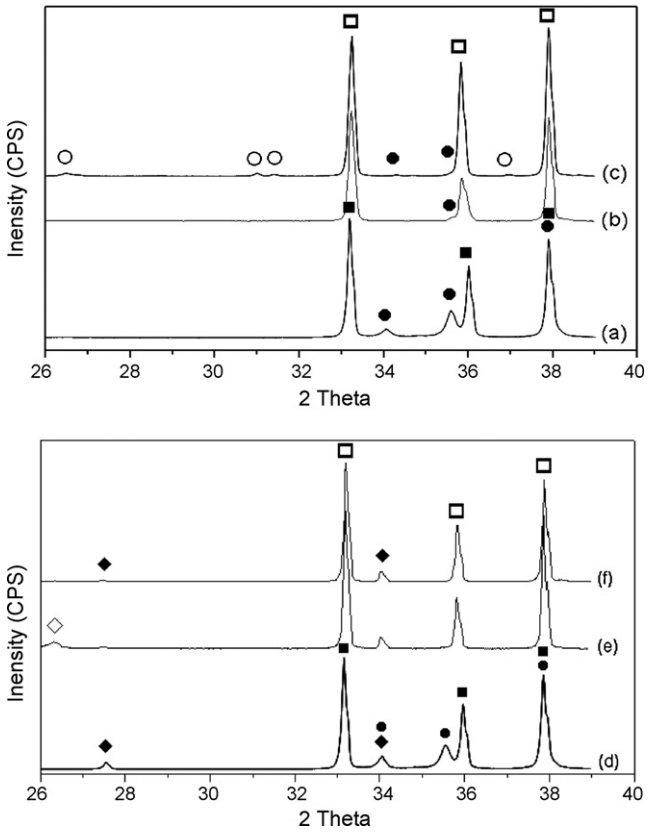

Fig. 3. XRD patterns of sintered samples (a) AS, raw powder mixture; (b) AS, 2000 °C; (c) AS, 2100 °C; (d) AST, raw powder mixture; (e) AST, 2100 °C and (f) ASTC, 2100 °C (■: AlN, ●: α-SiC, ♦: TiB_2, □: AlN–SiC solid solution, ◊: BN and ◯: unidentified peaks).

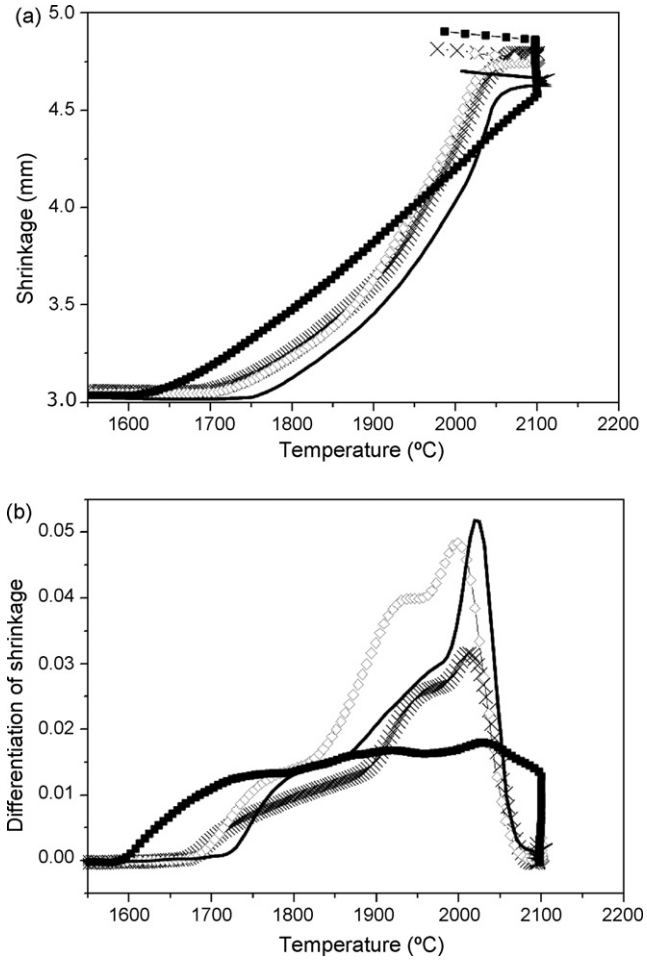

Fig. 4. (a) Shrinkage and (b) differentiation of shrinkage of samples with temperature in Ar (—:ATB4C, ■: STB4C, ◊: ASTB4C and ×: ASTBC). The samples were heat treated at 1500 °C for 30 min in vacuum before hot pressing at 2100 °C for 1 h in Ar (heating rate: 30 °C/min).

tives, densification of the AlN–SiC–TiB_2 system was completed during heating stage at 2030 °C by the application of carbon and boron or B_4C additives, and dense samples were obtained after the hot pressing at 2000 °C for 1 h (Table 3).

Differentiation of the shrinkage curve showed a three-step sintering behavior of the ASTBC and ASTB4C system (Fig. 4b). The same behavior occurred in the ATB4C system. On the other hand, the shrinkage behavior of the STB4C system was different from those of the above systems. Addition of SiC to the ATB4C system decreased the onset temperature of each step.

Fig. 5 shows TEM images of the ATB4C system sintered at 1930 and 2010 °C. TiB_2 was mostly placed between the boundaries of AlN grains. Intensive grain growth occurred at 2010 °C.

Fig. 6 shows the XRD data of the ASTBC and ASTB4C system after the sintering at different temperatures. Formation of solid solution did not strongly occur up to 1950 °C, while

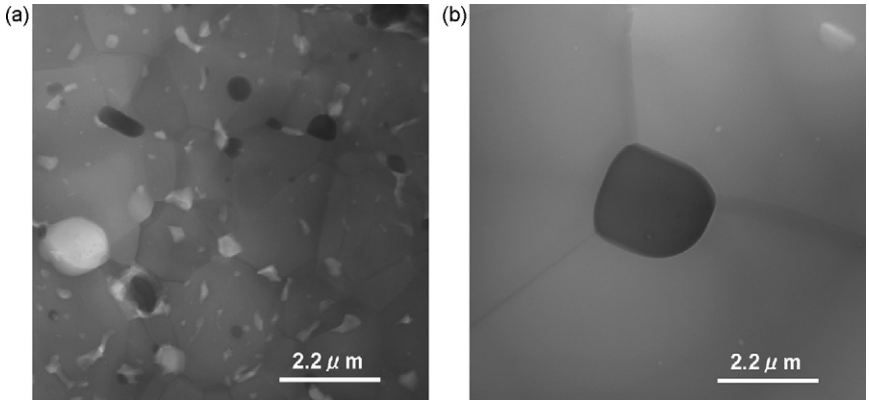

Fig. 5. TEM image of the ATB4C system hot pressed at (a) 1930 °C and (b) at 2010 °C (black: TiB_2, gray: AlN, white: pores formed during the sample preparation).

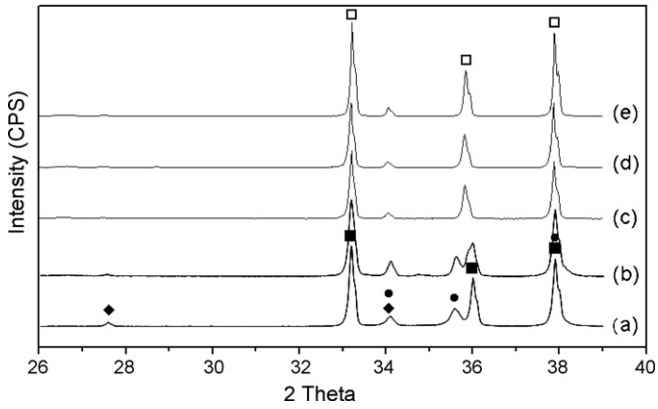

Fig. 6. XRD patterns of sintered samples (a) ASTB4C, raw powder mixture; (b) ASTBC, 1950 °C; (c) ASTBC, 2000 °C; (d) ASTBC, 2100 °C and (e) ASTB4C, 2100 °C (■: AlN, ●: α-SiC, ♦: TiB_2 and □: AlN–SiC solid solution).

the peaks of α-SiC disappeared nearly completely at and above 2000 °C.

3.3. Mechanical properties and thermal conductivity

Table 4 lists some mechanical properties of the dense specimens (>98% relative density). Among the tested systems, the ASTC system had the highest Young's modulus, hardness and fracture toughness. The addition of up to 5 wt% TiB_2 did not have strong effect on the mechanical properties of the near-stiochiometric AlN–SiC solid solution. Crack deflection occurred near TiB_2 grains (Fig. 7).

The thermal conductivity of the ASTB4C system hot pressed at 2100 °C under 45 MPa pressure was 22.9 W/(m °C). Relative density of the tested specimen was 99.9%.

4. Discussion

4.1. Thermal decomposition

Because Al_2O_3 and SiO_2, which present at the surface of AlN and SiC powder, form liquid phase and may promote densification of AlN–SiC system by liquid phase sintering, their decomposition may directly affect the densification behavior and high temperature properties of AlN–SiC system.

The weight loss of the AS system below 1500 °C (Fig. 1a) was partly due to the decomposition of SiO_2 by the reaction with carbon compound originated from the crucible and furnace.[17]

$$SiO_{2(s)} + 3C_{(s)} \rightarrow SiC_{(s)} + 2CO_{(g)}. \quad (1)$$

Table 4
Young's modulus, hardness and fracture toughness of dense samples

Sintering condition	Young's modulus (GPa)	Hardness (GPa)	Fracture toughness (MPa $m^{1/2}$)
ASTC, 2100 °C	324.2	19.5	4.2
ASTBC, 2000 °C	320.5	18.7	3.8
ASTB4C, 2100 °C	312.9	18.2	3.7

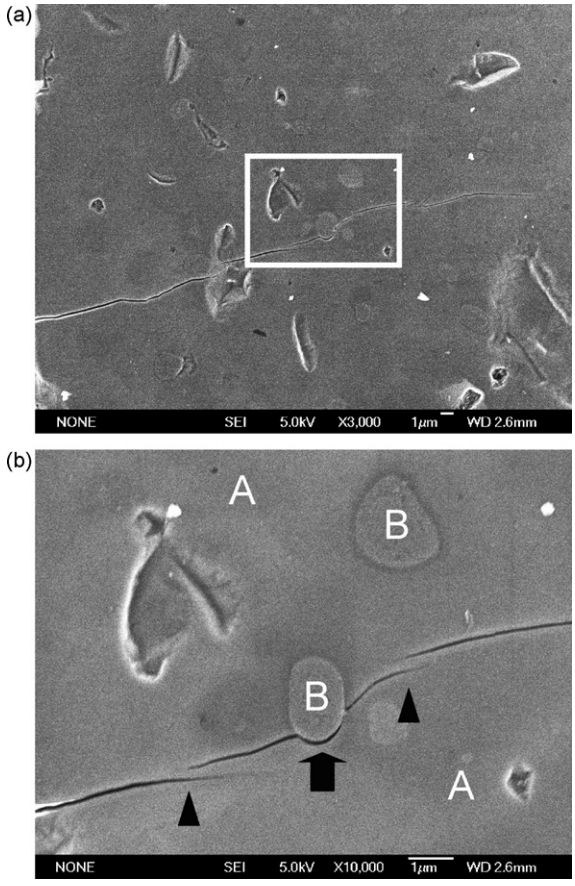

Fig. 7. Crack path in the ASTC system sintered at 2100 °C (A: solid solution, B: TiB_2, ▲: crack branching, ➡: intergranular fracture).

The onset temperature of reaction (1) was reported to be at around 1200 °C.[18] The reaction was completed at 1380 °C during slow heating (heating rate: 3 °C/min) when sufficient amount of carbon was added (Fig. 1b). The difference of weight loss between the ATB4C and ASTB4C system also originated from the reaction of SiO_2 with carbon, thus the disparity did not occur above 1380 °C (Fig. 1c and d). However, due to the lack of carbon, presumably reaction (2) occurred in the AS system during annealing at 1500 °C, the onset temperature of which was reported to be ~1500 °C.[19]

$$2SiO_{2(s)} + SiC_{(s)} \rightarrow 3SiO_{(g)} + CO_{(g)}. \quad (2)$$

The weight loss of the ATB4C system at 1500 °C (Fig. 1c) was mainly due to the reaction between Al_2O_3 and carbon.[20]

$$Al_2O_{3(s)} + 2C_{(s)} \rightarrow Al_2O_{(g)} + 2CO_{(g)}, \quad (3)$$

$$2Al_2O_{3(s)} + 3C_{(s)} \rightarrow Al_4O_4C_{(s)} + 2CO_{(g)}. \quad (4)$$

Zhang and Yamaguchi reported that both reactions actively occurred at 1500 °C in Ar.[20] Inoue et al. reported that formation of Al_4O_4C, which is thermally stable up to 1890 °C, became intensive at and above 1500 °C in vacuum.[21] In fact, certain amount of oxides remained in the AST and ASTC system after annealing at 1500 °C (Table 2), although TGA data informed that SiO_2 at the surface of SiC powder should be mostly removed after the annealing when carbon is contained in the powder mix-

ture (Fig. 1b). The result indicated the formation of Al_4O_4C after annealing at 1500 °C. Decomposition of Al_2O_3 by the reaction with AlN becomes intensive above 1750 °C,[22] thus the reaction did not contribute to the weight loss during annealing of the AST and ASTC system at 1500 °C.

The decrease of the surface area of the AST and ASTC system after the annealing at 1500 °C (Table 2) implies that for the densification of the annealed powder mixture, a higher temperature and/or pressure will be required compared to the case without the treatment. The surface area of the ASTC system was very high due to the decomposition of phenolic resin and the formation of porous carbon having high surface area during drying at 150 °C in vacuum before BET measurement.

4.2. Densification and phase analysis

The densification of AlN–SiC system generally requires high temperature and pressure (hot pressing at 2000–2300 °C).[23] In the present study, weight loss due to the decomposition of AlN was strongly enhanced at 2200 °C in Ar (2–3% at 2000 °C, 3.5–4.5% at 2100 °C and 8.3–9.2% at 2200 °C).[24] Consequently, the sintering temperatures applied in the following experiments were set at and below 2100 °C.

The first shrinkage of the AS system (Fig. 2b) is mainly due to the formation of a liquid phase composed of Si–Al–O–N. The onset temperature of the first shrinkage was similar to the eutectic temperature of Al_2O_3–SiO_2 system (1595 °C).[25] In addition, Al_2O_3 on the surface of AlN powder was reported to enhance the densification of AlN above 1500–1650 °C by forming oxynitrides.[26] On the other hand, SiO_2 in the liquid phase decomposed strongly above 1700 °C by reaction (2). Aluminum oxynitride also decomposed by the reaction with carbon species.[27] Consequently, densification of the AS system became sluggish above 1750 °C. The first shrinkage should be suppressed when SiO_2 and aluminum oxynitride are removed below the onset temperature of initial shrinkage, which did occur in the ASTC system by the addition of carbon (Fig. 2a).

The second shrinkage of the AS system at 1970–2060 °C (Fig. 2b) was presumably due to the formation of a liquid phase mainly composed of Al_2O_3. Impurities such as carbon might slightly decrease the melting temperature of Al_2O_3 (2053 °C).[12] Al_2O_3 was reported to decomposes by the reaction with SiC above 1700–2000 °C as follows;[19]

$$SiC_{(s)} + Al_2O_{3(s)} \rightarrow SiO_{(g)} + Al_2O_{(g)} + CO_{(g)}. \quad (5)$$

Consequently, the second shrinkage diminished above 2060 °C due to the lack of a liquid phase. The above discussion explains why the densification of the AS system occurred at 2000 °C, while the shrinkage was not observed at 2100 °C.

Pan et al. reported that the reaction mechanism between AlN and SiC to form solid solution was mainly governed by evaporation and condensation of AlN.[28] Since the mechanism does not induce shrinkage of the specimen in spite of large mass transfer, formation of solid solution was nearly completed in the AS system without densification.[29]

The relative density of the AST system was much higher than that of the AS system after hot pressing at 2100 °C. A possible mechanism to explain the difference is liquid phase sintering by the melt of Al_2O_3.[12] AlN reacts with B_2O_3 on TiB_2 to form Al_2O_3 and BN.[30]

$$2AlN_{(s)} + B_2O_{3(l)} \rightarrow Al_2O_{3(s)} + 2BN_{(s)}. \quad (6)$$

The reaction presumably increased the amount of Al_2O_3, thus enhanced liquid phase sintering of the AST system. Formation of BN by reaction (6) was observed in the AST system (Fig. 3e).

The low shrinkage of the ASTC system up to 1850 °C (Fig. 2a) was due to the decomposition of SiO_2 and aluminum oxynitride during heating. The densification above 1850 °C was presumably dominated by a liquid phase composed of aluminum, oxygen and carbon. Inherent Al_2O_3 in AlN reacted with carbon to form Al_4O_4C. The eutectic temperature of Al_2O_3–Al_4O_4C system was reported to be 1850 °C,[31] which was the same with the onset temperature of shrinkage of the ASTC system (1850 °C, Fig. 2b).

The three-step sintering behavior shown in Fig. 4(b) indicated that boron, B_4C and carbon additives induced the shrinkage of AlN, thus promoted the densification of AlN–SiC–TiB_2 system. TEM images of the ATB4C informed that growth of the AlN grains was enhanced at the third step during the densification (Fig. 5).

4.3. Mechanical properties and thermal conductivity

While Young's modulus (E) and Vickers hardness (Hv) of AlN–SiC solid solutions have been reported to be nearly proportional to the mixing ratio of AlN (E: 275 GPa, Hv: 14 GPa) [13,32] and SiC (E: 401 GPa, Hv: 33 GPa),[33] their fracture toughness did not have clear relationship with mixing ratio.[23] The Young's modulus, fracture toughness and hardness of near-stoichiometric AlN–SiC solid solution (AlN content: 65.4–74 wt%)[23,33] was reported to be 307[34]–352 GPa,[33] 3.3[23]–5.7 MPa $m^{1/2}$,[35] and 17–21 GPa,[23,36] respectively.

Reports about the mechanical properties of the AlN–SiC–TiB_2 system are scarce. The results of the present research indicate that the addition of up to 5 wt% TiB_2 did not have strong effect on the mechanical properties of near-stiochiometric AlN–SiC solid solution, in spite of the fact that the Young's modulus and hardness of TiB_2 (367, 34 GPa)[23] are higher than those of the solid solution.

Crack deflection occurred in the ASTC system due to the presence of residual stress induced by the different CTE value between the solid solution (4.6×10^{-6}/°C) and TiB_2 (6.39×10^{-6}/°C).[13,23] The fracture toughness of AlN and SiC has been reported to be improved by the incorporation of TiB_2.[37,38] In both cases, crack deflection was enhanced by the residual stress originated from the difference of CTE between the matrix and TiB_2. Fracture toughness of the AlN–SiC solid solution is also expected to be improved in case sufficient amount of TiB_2 is incorporated, but the addition did not distinctly improve the property when the amount was fixed to 5 wt%.

The thermal conductivity of the ASTB4C system was similar to that of AlN–SiC solid solution reported by Rafaniello et al. (20 W/(m °C), AlN content: 75 wt%).[23] The thermal conductivity of AlN and SiC were reported to be 200 and 41.7 W/(m °C), respectively, but rapid decrease of the value has been observed in the solid solution.[39,40] Landon and Thevenot attributed the reason to the self collision of phonons and interactions of phonons with defects in the solid solution.[32] Addition of up to 5 wt% TiB_2 did not strongly improve the thermal conductivity of the AlN–SiC solid solution although the value of TiB_2 (100 W/(m °C)) was much higher than that of the solid solution.[41]

5. Summary and conclusion

SiO_2 and Al_2O_3 induced densification of the AlN–SiC system above 1600 °C. The former phase could be removed by carbothermal reduction process, while the latter one remained and affected the densification behavior of the system. Densification of the AlN–SiC system did not intensively occur at 2100 °C with 20 MPa pressure in case the temperature range of the second shrinkage (1970–2060 °C) passed rapidly during heating. TiB_2 induced densification of the AlN–SiC system above 2050 °C. Dense specimens with high relative density (>98%) could be obtained at 2000 °C by the application of C and B or B_4C as sintering additives. The additives promoted the densification of AlN in the systems. Young's modulus, hardness, fracture toughness and thermal conductivity of the AlN–SiC–TiB_2 system containing 5 wt% TiB_2 were similar to those of the AlN–SiC system.

References

1. Kimmel, J., Miriyala, N., Price, J., More, K., Tortorelli, P., Eaton, H. *et al.*, Evaluation of CFCC liners with EBC after field testing in a gas turbine. *J. Eur. Ceram. Soc.*, 2002, **22**, 2769–2775.
2. Weidenmann, K. A., Rixecker, G. and Aldinger, F., Liquid phase sintered silicon carbide ceramics having remarkably high oxidation resistance in wet air. *J. Eur. Ceram. Soc.*, 2006, **26**, 2453–2457.
3. Baxter, D., Bellosi, A. and Monteverde, F., Oxidation and burner rig corrosion of liquid phase sintered SiC. *J. Eur. Ceram. Soc.*, 2000, **20**, 367–382.
4. Shimada, S. and Aketo, T., High-temperature oxidation at 1500 °C and 1600 °C of SiC/Graphite coated with Sol–Gel-derived HfO_2. *J. Am. Ceram. Soc.*, 2005, **88**(4), 845–849.
5. Lavrenko, V. A., Desmaison-Brut, M., Panasyuk, A. D. and Desmaison, J., Features of corrosion resistance of AlN–SiC ceramics in air up to 1600 °C. *J. Eur. Ceram. Soc.*, 1998, **18**, 2339–2343.
6. Lavrenko, V. A., Baxter, D. J., Panasyuk, A. D. and Brut, M. D., High-temperature corrosion of AlN-based composite ceramics in air and in combustion products of commercial fuel. 1. Corrosion of ceramic composites in the AlN–SiC system in air and in combustion products of kerosene and diesel fuel. *Powder Metall. Metal Ceram.*, 2004, **43**(3–4), 179–186.
7. Lavrenko, V. A., Baxter, D. J., Panasyuk, A. D., Brut, M. D., Fenard, E. and Pavlikov, V. N., High-temperature corrosion of AlN-based composite ceramic in air and in combustion products of commercial fuel. 2. Corrosion of ceramic composites in the AlN–SiC–TiB_2 system in air and in combustion products of kerosene and diesel fuel. *Powder Metall. Metal Ceram.*, 2004, **43**(5–6), 295–303.
8. Reser, M. K., ed., *Phase Diagrams for Ceramists*. The American Ceramic Society, Columbus, OH, 1964 [Fig. 771].
9. Rafaniello, W., Cho, W. K. and Virkar, A. V., Fabrication and characterization of SiC–AlN alloys. *J. Mater. Sci.*, 1981, **16**, 3479–3488.
10. Huang, J. L. and Jih, J. M., Investigation of SiC–AlN system: part 1. microstructure and solid solution. *J. Mater. Res.*, 1995, **10**(3), 651–658.
11. Stobierski, L. and Gubernat, A., Sintering of silicon carbide, 2. Effect of boron. *Ceram. Inter.*, 2003, **29**, 355–361.
12. Lide, D. R., ed., *CRC Handbook of Chemistry and Physics*. Taylor & Francis Group, Boca Raton, 2005, pp. 4-6–4-84.
13. Shaffer, P. T. B., ed., *Plenum Press Handbook of High-Temperature Materials, No. 1, Materials Index*. Plenum Press, New York, 1964, pp. 55–57.
14. Zhou, Y., Tanaka, H., Otani, S. and Bando, Y., Low-temperature pressureless sintering of α-SiC with Al_4C_3–B_4C–C additions. *J. Am. Ceram. Soc.*, 1999, **82**(8), 1959–1964.
15. Japanese Industrial Standard, *Testing Methods for Fracture Toughness of Fine Ceramics*. Japanese Standards Association, Tokyo, 1995 [JIS R 1607].
16. Cutler, I. B., Miller, P. B., Rafaniello, W., Park, H. K., Thompson, D. P. and Jack, K. H., New materials in the Si–C–Al–O–N and related systems. *Nature*, 1978, **275**, 434–435.
17. Hampshire, S. and Jack, K. H., In *Ceramic Components for Engines*, ed. S. Somoya, E. kanai and K. Ando. KTK Scientific, 1984, pp. 350–357.
18. Colombo, P. and Modesti, M., Silicon oxicarbide foams from a silicon preceramic polymer and polyurethane. *J. Sol–Gel Sci. Tech.*, 1999, **14**, 103–111.
19. Grande, T., Sommerset, H., Hagen, E., Wiil, K. and Einarsrud, M. A., Effect of weight loss on liquid-phase-sintered silicon carbide. *J. Am. Ceram. Soc.*, 1997, **80**(4), 1047–1052.
20. Zhang, S. and Yamaguchi, A., Hydration resistances and reactions with CO of Al_4O_4C and Al_2OC formed in carbon-containing refractories with Al. *J. Ceram. Soc. Jpn.*, 1996, **104**(5), 393–398.
21. Inoue, K. and Yamaguchi, A., Synthesis of Al_4SiC_4. *J. Am. Ceram. Soc.*, 2003, **86**(6), 1028–1030.
22. Kim, N. H., Fun, Q. D., Komeya, K. and Meguro, T., Phase reaction and sintering behavior in the pseudoternary system AlN–Y_2O_3–Al_2O_3. *J. Am. Ceram. Soc.*, 1996, **79**, 2645–2651.
23. Rafaniello, W., Plichta, M. R. and Virkar, A. V., Investigation of phase stability in the system SiC–AlN. *J. Am. Ceram. Soc.*, 1983, **66**(4), 272–276.
24. Taylor, K. M. and Lenie, C., Some properties of aluminum nitride. *J. Electrochem. Soc.*, 1960, **107**(4), 308–314.
25. Aramaki, S. and Roy, R., The Mullite-corundum boundary in the systems MgO–Al_2O_3–SiO_2 and CaO–Al_2O_3–SiO_2. *J. Am. Ceram. Soc.*, 1959, **42**(12), 644–645.
26. Sakai, T., Kuriyama, M., Inukai, T. and Kizima, T., Effect of the oxygen impurity on the sintering and the thermal conductivity of AlN polycrystal. *Yogyo-Kyokai-Shi*, 1978, **86**(4), 30–35.
27. Amadeh, A., Labbe, J. C., Laimeche, A. and Quintard, P., Influence of boron nitride and carbon additives on the behaviour of sintered AlN in a steelmaking environment. *J. Eur. Ceram. Soc.*, 1996, **16**(4), 403–408.
28. Pan, Y., Tan, S., Jiang, D., Qiu, J., Kawagoe, M. and Morita, M., In-situ characterization of SiC–AlN multiphase ceramics. *J. Mater. Res.*, 1999, **34**, 5357–5360.
29. Kingery, W. D., Bowen, H. K. and Uhlmann, D. R., *Introduction to Ceramics* (*2nd ed.*). John Wiley & Sons, New York, 1976, pp. 470–474.
30. Kurita, S., Zeng, Z. Q., Takabe, H. and Morinaga, K., Reaction and phase relations in the AlN–B_2O_3 system. *Mater. Trans. JIM*, 1994, **35**(4), 258–261.
31. Qiu, C. and Matselaar, R., Phase relations in the aluminum carbide–aluminum nitride–aluminum oxide system. *J. Am. Ceram. Soc.*, 1997, **80**(8), 2013–2020.
32. Landon, M. and Thevenot, F., The SiC–AlN system: influence of elaboration routes on the solid solution formation and its mechanical properties. *Ceram. Int.*, 1991, **17**, 97–110.
33. Ruh, R., Zangvil, A. and Barlowe, J., Elastic properties of SiC, AlN, and their solid solutions and particulate composites. *Am. Ceram. Soc. Bull.*, 1985, **64**(10), 1368–1373.
34. Yamada, Y., Kawasaki, A., Li, J. F., Taya, M. and Watanabe, R., Young's modulus and fracture toughness of SiC–AlN composite. *J. Jpn. Inst. Metals*, 1992, **56**(9), 1078–1086.
35. Li, F. F. and Watanabe, R., Mechanical properties of SiC–AlN ceramic composites. In *Transactions of the Materials Research Society of Japan*, *Vol 3*,

ed. S. Somiya, M. Doyama, M. Hasegawa and Y. Agata. The Materials Research Society of Japan, Kawasaki, 1992, pp. 74–85.
36. Tangen, I. L., Yu, Y., Grande, T., Mokkelbost, T., Hoier, R. and Einarsrud, M. A., Preparation and characterization of aluminium nitride–silicon carbide composites. *Ceram. Int.*, 2004, **30**(6), 931–938.
37. Zhang, X. Y., Tan, S. H. and Jiang, D. L., AlN–TiB_2 composites fabricated by spark plasma sintering. *Ceram. Int.*, 2005, **31**(2), 267–270.
38. Yamada, K., Matsubara, M. and Matsumoto, M., Toughening mechanism of particle dispersed SiC composites. *J. Ceram. Soc. Jpn.*, 1998, **106**(10), 1084–1091.
39. Iwamoto, N., Fundamental properties of AlN. In *Transactions of the Materials Research Society of Japan*, *Vol 3*, ed. S. Somiya, M. Doyama, M. Hasegawa and Y. Agata. The Materials Research Society of Japan, Kawasaki, 1992, pp. 85–179.
40. Liethschmidt, K., Silicon carbide. In *Ullmann's Encyclophedia of Industrial Chemistry*, *Vol A23*, ed. B. Elvers, S. Hawkins, W. Russey and G. Schultz. VCH publischers Inc., Weinheim, 1993, pp. 749–759.
41. Yih, P. and Chung, D. D. L., Titanium diboride copper–matrix composites. *J. Mater. Sci.*, 1997, **32**, 1703–1709.